VOL. 3, NO.12 Dec, 2012 ISSN 2079-8407
Journal of Emerging Trends in Computing and Information Sciences

http://www.cisjournal.org

Performance Prediction of Carbon Nano Tube Dipole Antenna Using the Complex Permittivity Approach

[1] Moretadha J. Kadhom, [2] Jaber S. Aziz, [3] R. S. Fyath
[1] College of Engineering, University of Baghdad, Baghdad, Iraq
[2, 3] College of Engineering, Alnahrain University, Baghdad, Iraq
[1] Moretadha1982@yahoo.com, [2] jsaziz53@yahoo.com, [3] rsfyath@yahoo.com

ABSTRACT

The concept of the effective conductivity of carbon nanotube (CNT) material is introduced and used to investigate the radiation characteristics of various configurations of CNT dipole antenna. The concept takes into account the frequency dependent complex permittivity of the CNT material and lends itself to a virtual CNT dipole suitable for adaptation in conventional antenna theory and in commercial electromagnetic software solvers. Simulation results related to single–wall, multi-wall, and bundle CNT dipole antennas are presented using CST software package to show the effect of various geometric parameters on antenna performance. The problem of antenna feeding is also discussed and leads to the proposal of using CNT transmission line feeder.

Keywords: *Carbon nanotube, Nanoantenna*

1. INTRODUCTION

Since the discovery of the unique antenna from carbon nanotube (CNT) in 2004, there has been more strong interest in nanoantenna, and much concerning their lengths from nanometer scale to centimeters. This leads to a topic considering CNTs for sub-millimeter, millimeter and centimeter wave antenna applications [1]. Therefore, CNTs have been investigated nowadays as antennas in various areas-communication between nano devices and macroscopic world, nano interconnect, fiber communication, aircraft and space communication systems. Their advantages are the small sizes, light weight, and remarkable electric properties [2]. Carbon nano tubes are tubular structures typically of nanometer diameter and many microns in length. They are unusual because of their very small diameters, which can be as small as 0.4 nm and contain only 10 atoms around the circumference, and because the tubes can be only one atom in thickness. The aspect ratio (length/diameter) can be very large (greater than 10^4), thus leading to a prototype one-dimensional system [3]. This aspect ratio can be accepted when one talks about the CNT application in antenna field. Therefore it is necessary to study the electromagnetic properties of this material.

The performance of CNT dipole antennas has been investigated by many researchers using comprehensive numerical techniques. In 2005, Hanson [4] investigated fundamental properties of dipole transmitting antennas formed by CNTs via a classical Hallén's- type integral equation (HIE), based on a quantum mechanical conductivity. In 2006, Hao and Hanson [5] presented a model for electromagnetic scattering from infinite planar arrays of finite-length metallic CNTs, and isolated nanotubes, in the lower infrared radiation (IR) bands. The scattered field has been predicted using a semiclassical formulation based on a periodic Green's function for the array, and a quantum conductance function for the CNTs. In 2006, Hanson [6] studied the current on an infinitely-long CNT antenna fed by a delta-gap source using Fourier transform technique. The CNT has been modeled as an infinitely-thin tube characterized by a semi-classical conductance. The CNTs current has been compared with the current on solid and tubular copper antennas having similar or somewhat larger radius values. In 2006, Hao and Hanson [7] investigated the characteristics of armchair CNT dipole antennas in the infrared and optical regime using classical electromagnetic HIE, and an axial quantum mechanical conductance function for the tube. In 2006, Burke et al. [8] presented quantitative predictions of the performance of nanotubes and nanowires as antennas, including the radiation resistance, the input reactance and resistance, and antenna efficiency, as a function of frequency and nanotube length. They developed models for both far-field antenna patterns as well as near-field antenna-to-antenna coupling. Also, a circuit model has been developed for a transmission line made of two parallel nanotubes. Finally, an analog of HIE appropriate for single-wall CNT (SWCNT) antennas has been derived. In 2007, Hao and Hanson [9] developed a model for optical scattering from planar arrays of finite-length single-wall metallic CNTs. The scattered field has been predicted using a periodic Green's function for the array, which includes all electromagnetic interactions, and a quantum conductance function $g(\omega)$ for the CNTs. In 2007, Wang et al. [1] investigated by simulation the geometric structure and the terahertz (THz)/IR characteristics of CNTs dipole antenna arrays using finite integral methods. In 2007, Maksimenko et al. [10] presented a theory of the metallic a chiral CNT as a vibrator antenna. The Leontovich–Levin integral equation (IE) method has been extended to the case of CNTs. Integral equations for the finite-length CNT and CNT bundles were solved numerically in the integral operator quadrature approximation with the subsequent

transition to the finite-order matrix equation. In 2008, Fichtner et al. [11] investigated the characteristics of small CNT dipole antennas on the basis of the thin wire HIE. A surface impedance model for the CNT was adopted to account for the specific material properties resulting in a modified kernel function for the integral equation. In 2010, Nemilentsau et al. [12] examined lateral resolution of CNT tip with respect to an ideal electric dipole representing an elementary detected object. A Fredholm IE of the first kind has been formulated for the surface electric current density induced on SWCNT by the electromagnetic field due to an arbitrarily oriented electric dipole located outside the tube. In 2011, Berres and Hanson [13] analyzed isolated, infinitely long multi-wall CNTs (MWCNTs) interacting with electromagnetic waves in the microwave and far-infrared frequency regime using a semi-classical approach. In 2011, Choi and Sarabandi [14] evaluated the performance of bundled carbon nanotubes (BCNTs) as a conducting material for the fabrication of antennas in the THz frequency range and above. Numerical simulations using the method of moments (MoM) and the mixed potential integral equation (MPIE) have been performed to quantify radiation efficiencies of resonant strip antennas composed of BCNTs and thin gold films.

In this work, a virtual CNT model is developed to be used with commercial software packages to deduce the performance of various CNT antenna configurations. This opens the door to deal with all configurations of CNTs antennas not just the dipole one.

2. THEORETICAL FRAMEWORK

In the low-frequency regime, below optical interband transitions ($\omega < (\upsilon_F/r)$), where υ_F is the Fermi velocity and r is the radius of the CNT, the conductivity of armchair or zigzag SWCNT is given by [5]

$$g(\omega) = -j\frac{2e^2\upsilon_F}{\pi^2\hbar r(\omega - j\nu)} \qquad \dots(1)$$

where e is the electron charge and $\hbar$ is the reduced Planck's constant ($\hbar = 1.05457266 \times 10^{-34}$ J.s), ν is the phenomenological relaxation frequency ($\nu = \tau^{-1} = 6\mathrm{T}/r$), T is temperature in Kelvin, and τ is relaxation time. Further, $\upsilon_F = 3\gamma_0 b/2\hbar$, with ($\gamma_0 = 2.7$ eV at low and middle IR frequencies and $b = 0.142$ nm is the interatomic distance in graphene.

The conductivity for armchair SWCNT tubes with various $m = n$ values, where m and n are the radius indices, is shown in Fig. 1. Equation 1 indicates that the conductivity is a complex quantity and therefore can be expressed as

$$g(\omega) = g_r(\omega) + jg_i(\omega) \qquad \dots(2a)$$

$$= |g(\omega)|e^{j\phi_g(\omega)} \qquad \dots(2b)$$

Where

$$g_r(\omega) = \frac{2e^2\upsilon_F}{\pi^2\hbar r}\frac{\nu}{\omega^2+\nu^2} \qquad \dots(3a)$$

$$g_i(\omega) = -\frac{2e^2\upsilon_F}{\pi^2\hbar r}\frac{\omega}{\omega^2+\nu^2} \qquad \dots(3b)$$

$$|g(\omega)| = \frac{2e^2\upsilon_F}{\pi^2\hbar r}\frac{\sqrt{\omega^2+\nu^2}}{\omega^2+\nu^2} \qquad \dots(4a)$$

$$\phi_g(\omega) = \tan^{-1}\left(\frac{\nu}{\omega}\right) - \frac{\pi}{2} \qquad \dots(4b)$$

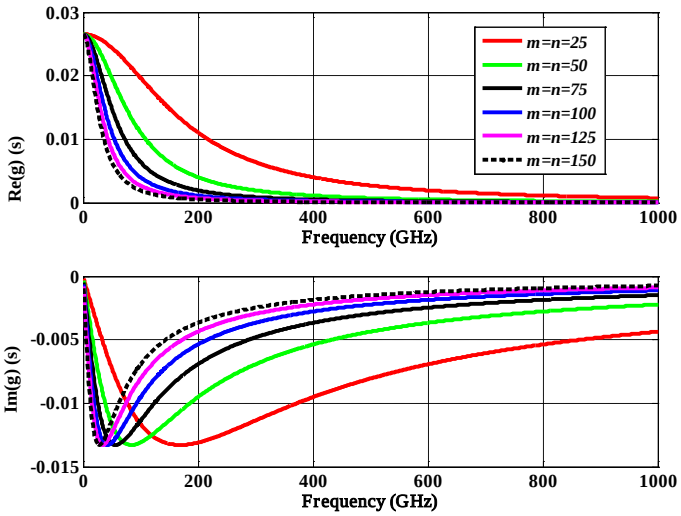

Fig 1: Conductivity of the armchair SWCNT for various $m = n$ values (i.e., various radius values) at T=300^{0}K.

One can note that the maximum values of $|g_r(\omega)|$ and $|g_i(\omega)|$ occur at $\omega = 0$ and $\omega = \nu$, respectively. At zero frequency, the conductivity is real and is given by

$$g(0) = \frac{2e^2\upsilon_F}{\pi^2\hbar r\nu} \qquad \dots(5)$$

For an armchair SWCNT with $m = n = 40$, and assuming $\upsilon_F = 9.71 \times 10^5\ m/s$, the quantum resistance is 2.2 k$\Omega/\mu m$ at T = 300^0K. The distributed impedance (Ω/m) of the SWCNT structure is given by [15]

$$Z_i = \frac{1}{2\pi r g} \qquad \dots(6a)$$

$$= \mathcal{R} + j\omega\mathcal{L}_k \qquad \dots(6b)$$

where

$$\mathcal{R} = \frac{\pi\hbar\nu}{4e^2\upsilon_F} = \frac{3}{2}\frac{\hbar\mathrm{T}}{e^2\upsilon_F r} \qquad \dots(7a)$$

$$\mathcal{L}_k = \frac{\pi\hbar}{4e^2 v_F} \quad \ldots(7b)$$

and $\mathcal{L}_k = \mathcal{R}\tau$. Here $\mathcal{R}$ and $\mathcal{L}_k$ are the per unit length (p.u.l) quantum resistance and kinetic inductance, respectively. Note that $\mathcal{R}$ is inversely proportional to CNT radius and proportional to temperature (when the effect of temperature on Fermi velocity is neglected). The value of L_k for $v_F = 9.71 \times 10^5\ m/s$ is $3.3\ \mathrm{n}H/\mu\mathrm{m}$ which is large value with respect to magnetic inductance in transmission line which has values near to $\mu = 0.4\pi\ \mathrm{p}H/\mu\mathrm{m}$. This emphasizes the domination of the inductance on the parameters of transmission line such as phase velocity, propagation constant, phase constant, and so on. This fact makes the CNT more attraction than the other materials since it has properties which are not satisfied in the other materials.

3. EFFECTIVE CONDUCTIVITY OF CNT

The unit of CNT conductivity g (as a hollow tube) is measured in Siemens (S), but the conductivity σ in Maxwell's equations is measured in (S/m). The reason for this difference is the geometry of the CNT which leads to considering it as a longitudinal geometry and the derivation of the CNT conductivity is based on this fact. In contrast, the metal wires are usually assumed to be a bulk and the physical geometry is assumed to be a transverse then the unit of the conductivity appeares to be (S/m). To solve this problem, the CNT is considered here as having an equivalent cylinder with the effective parameters in order to manipulate it simply with Maxwell's equations. This modification will encompass SWCNT and MWCNT antennas and can also be applied to the BCNT antenna.

3.1 SWCNT

As mentioned before, the conductivity of a SWCNT model was derived as one dimensional system, where the current is passing on the surface only. Now, assuming a uniform surface current density $\boldsymbol{K}$ for the SWCNT with radius r and line current density $\boldsymbol{I}$ passing through it, then $\boldsymbol{K}$ is defined as

$$\boldsymbol{K} = \frac{\boldsymbol{I}}{2\pi r} \quad \ldots(8)$$

One can model the CNT as a solid cylinder with radius r and line current density I to give the volume current density

$$\boldsymbol{J} = \frac{\boldsymbol{I}}{\pi r^2} \quad \ldots(9)$$

From eqns. 8 and 9, $\boldsymbol{J} = (2/r)\,\boldsymbol{K}$. Applying Ohm's law $\boldsymbol{J} = \sigma\boldsymbol{E}$ to the effective solid cylinder and $\boldsymbol{K} = g\boldsymbol{E}$ to the SWCNT leads to

$$\sigma = \frac{2}{r}g = -j\frac{4e^2 v_F}{\pi^2\hbar r^2(\omega - j\nu)} \quad \ldots(10)$$

Where eqn. 1 has been used. Here, the electric field $\boldsymbol{E}$ is assumed to be the same on the surfaces of hollow and solid cylinders and this assumption will give more confidence to this modeling since the electric field and the line current density are assumed constant. Thus, the factor $(2/r)$ may be considered as a transformation factor from the old to the new version.

The Drude model of the metal conductivity may be written as [4]

$$\sigma = -j\frac{e^2 {N_d}^3}{m_e(\omega - j\nu)} \quad \ldots(11)$$

where N_d is the number of electrons per m^3 and m_e is the mass of electron. Hence, the equivalent expresion for N_d in a SWCNT may be found as

$$N_{eq} = \left(\frac{4m_e v_F}{\pi^2\hbar r^2}\right)^{1/3} \quad \ldots(12)$$

Equation 12 shows that the electron density N_{eq} in the solid cylinder is inversely proportional to $r^{2/3}$. This inverse proportion may make a constraint on the electromagnatic properties of a SWCNT when the radius becomes large enough and the SWCNT seems to be empty with carriers which are mainly responsible for the electric conduction. To explain this, the values of N_{eq} are calculated for a SWCNT with several radii as shown in Table 1. The results are to be compared with electron density of copper which equals to 8.46×10^{28} electron/m^3. It is seen from the table that all values of N_{eq} are very far from N_d and this may interprete the high impedance of a SWCNT when it is compared with the impedance of a metals. Thus the enough carriers for the conduction case do not exist in CNT.

According to this modeling, the input impedance of a SWCNT is equal to the input impedance of the effective cylinder

$$Z_i = \frac{L}{\pi\sigma\, r^2} = \frac{L}{2\pi g r} \quad (\Omega) \quad \ldots(13)$$

where L is the length of the CNT. This is not the input impedance of the SWCNT antenna as seen later.

Table 1: Dependence of effective carier density and radius of SWCNT.

$m=n$	r (nm)	N_{eq} (electron /m^3)	$m=n$	r (nm)	N_{eq} (electron /m^3)
10	0.67	1.9489×10^{9}	60	4.06	5.9023×10^{8}
20	1.35	1.2277×10^{9}	70	4.74	5.3258×10^{8}
30	2.03	9.3693×10^{8}	80	5.42	4.8722×10^{8}
40	2.71	7.7342×10^{8}	90	6.10	4.5043×10^{8}
50	3.39	6.6651×10^{8}	100	6.78	4.1988×10^{8}

3.2 MWCNT

The MWCNT consists of multiple co-centric SWCNTs, where the distance between each tube wall is approximately 0.34 nm, which is the distance between interatomic layers of graphite (i.e., graphene sheets). The number of tube walls for an MWCNT can vary anywhere from 2 to several hundred. From the emerging literature it becomes clear that for far-infrared applications, individual SWCNTs have losses that are too large (associated with their extremely small radius) to serve as antennas or interconnects [13].

As in a SWCNT, the MWCNT is suffering from the approach of measuring the conductivity which is considered as the main problem when these materials are applied for the antenna applications.

If only the longitudinal current is assumed, then the current in each CNT shell of the MWCNT (Fig. 2) is approximated as

$$I_n = 2\pi r_n g_n E_n , \qquad n = 1, 2, \dots, N \quad \dots (14)$$

where E_n, g_n, and r_n are the surface longitudinal electric field, conductivity, and radius, respectively, for the n^{th} wall and N is the number of tubes. Since the distance between neighboring shells is very small and assuming no current passing between the neighboring shells, then $E_n = E$ for all values of n and the total current is

$$I = \sum_{n=1}^{N} I_n = 2\pi E \quad \dots (15)$$

For the effective solid cylinder of radius r_N, the longitudinal current is given by

$$I = \pi r_N^2 \sigma E \quad \dots (16)$$

which is assumed to be an equivalent to the current in eqn. 15. Therefore,

$$\sigma = \frac{2}{r_N^2} \sum_{n=1}^{N} r_n g_n \quad \dots (17a)$$

$$= \frac{-j4e^2 v_F}{\pi^2 \hbar r_N^2} \sum_{n=1}^{N} \frac{1}{(\omega - j\nu_n)} \quad \dots (17b)$$

Generally, $\nu_n = 6\mathrm{T}/r_n$ and therefore $\nu_1 \neq \nu_2 \neq \nu_3 = \cdots$. If the relaxation frequency is assumed for simplicity to be the same for all tubes, then the conductivity of MWCNT can be simplified to

$$\sigma = \frac{2N}{r_N} g_N = N\sigma_N \quad \dots (81)$$

where σ_N is the effective conductivity of the N^{th} tube. In the view of electrical circuit, the effective solid cylinder of a MWCNT behaves as an equivalent resistance for N parallel equal resistances.

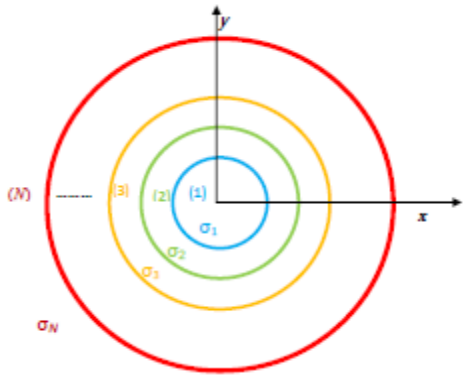

Fig 2: Schematic representation of the MWCNT cross section.

4. CNT COMPLEX PERMITTIVITY

The concept of the effective conductivity can be generalized to other quantities such as permittivity and permeability which are considered as main parameters in Maxwell's equations. If the relative permeability is assumed to be unity in all types of CNT then the concern is around the permittivity. The effective conductivity of the CNT is generally a complex quantity and can be expressed for SWCNT or MWCNT as

$$\sigma = \sigma_r + j\,\sigma_i \quad \dots (19)$$

where σ_r and σ_i are, respectively, the real and imaginary parts of the effective conductivity measured by (S/m). Therefore, from Maxwell's equations one can show that the real and imaginary parts of the relative complex permittivity

$$\varepsilon_c = \acute{\varepsilon}_c - j\acute{\varepsilon}_c \quad \dots (20)$$

can be expressed as

$$\acute{\varepsilon}_c = \varepsilon_{rel} + \frac{\sigma_i}{\omega\varepsilon_0} \quad \dots (21a)$$

$$\acute{\varepsilon}_c = \frac{\sigma_r}{\omega\varepsilon_0} \quad \ldots(21b)$$

Here ε_{rel} is the relative permittivity of the CNT material and ε_0 is the permittivity of the vacuum. If the imaginary part of the effective conductivity is assumed to be zero then the real part of the complex permittivity $\acute{\varepsilon}_c$ is equal to the relative permittivity as in metals such as a copper and gold (low frequency regime).

The Drude model in term of the relative permittivity of the metals can be expressed as [16]

$$\varepsilon_c(\omega) = \varepsilon_{rel} - \frac{\omega_p^2}{\omega(\omega - j\,\nu_{coll})} \quad \ldots(22)$$

where ω_p is the plasma frequency which is in CNT is found to be

$$\omega_p = \frac{2e}{\pi r}\sqrt{\frac{\upsilon_F}{\varepsilon_0 \hbar}} \quad \ldots(23)$$

and ν_{coll} is the collision frequency in metals and assumed as the same as the relaxation frequency ν in CNTs. For the CNT material with r=2.71 nm (m=n=40), the values of $f_p = \omega_p/2\pi$ and ν are found to be 1212 and 0.77 THz, respectively. This means that the CNT will receive the signal of this frequency and beyond as known from the plasma theory. If one assumes a large SWCNT radius with $r = 67$ nm (m=n=1000), then plasma frequency of a SWCNT material is 48.481 THz which is equivalent to a receiving antenna of length of 3.1 μm.

In conjunction of complex permittivity with plasma frequency, eqns. 21a and b can be rewritten in term of ω_p as

$$\acute{\varepsilon}_c = \varepsilon_{rel} + \frac{{\omega_p}^2}{\omega^2 + \nu^2} \quad \ldots(24a)$$

$$\acute{\varepsilon}_c = \frac{{\omega_p}^2 \nu}{\omega(\omega^2 + \nu^2)} \quad \ldots(24b)$$

As a result, the CNT material can be modeled with either eqn. 21 or 23 where both equations give the same results. Figure 3 shows the values of $\acute{\varepsilon}_c$ and $\acute{\varepsilon}_c$ for a SWCNT having $r = 2.71$ nm with $\nu/2\pi = 123.24$ GHz.

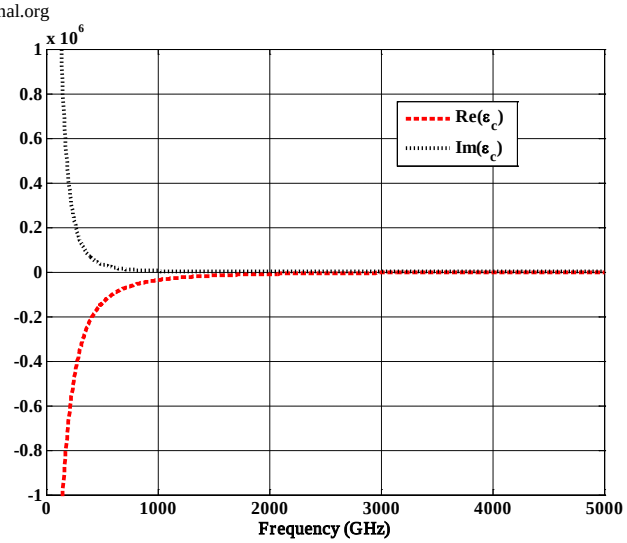

Fig 3: Real and imaginary parts of the complex permittivity of SWCNT with (m=n=40).

5. MODELING OF SWCNT ANTENNA USING COMPLEX PERMITTIVITY APPROACH

There are several methods for the investigation of the properties of the CNT antenna. The transmission line method [8] assumes the SWCNT antenna as a flared transmission line. The parameters of a transmission line are generalized to the SWCNT antenna. This method is capable of simple understanding of the effect of plasmon wavelength in CNT properties which is attributed to the existing kinetic inductance and quantum capacitance. Another method considers the SWCNT as a tubed cylinder with a longitudinal current only and the MoM is applied as a solver for the Maxwell's equations [4]. The mentioned references agree with the fact that SWCNT antenna does not resonate at $L = \lambda_0/2$ and multiples where λ_0 is the free space resonance wavelength. The SWCNT will resonate at $L = \lambda_{pc}/2$ and multiple, where λ_{pc} is the plasmon wavelength. Then, the resonance frequency is computed from $\upsilon_p = \lambda_{pc} f_r$ instead of $c = \lambda_0 f_r$ where υ_p, c, and f_r are the phase velocity, speed of light in free space, and resonance frequency, respectively. Usually, the phase velocity has values close to the Fermi velocity but not equal to it and it is estimated here because there is no exact formula in SWCNT. The previous explanation will support the results when the complex permittivity is used for modeling the CNT antenna shown in Fig. 4.

In the complex permittivity approach the numerical analysis depends on knowing the constitutive parameters of the antenna material. These parameters have been modeled in the previous section for CNT material and accordingly the CNT material becomes ready for the simulation. Because the CNT is non-magnetic material, the relative permeability is assumed to be unity such that $\mu = \mu_0$ where μ is the permeability of CNT and μ_0 is the

free space permeability. In this work, the CNT material is set up as a new material in CST environment with normal type. Discrete values of $\acute{\varepsilon}_c$ and $\acute{\varepsilon}_c$ are tabulated in dielectric dispersion fit window and computed using MATLAB. The frequency range is set up from 1 to 5000 GHz with 1 GHz frequency separation between two successive samples.

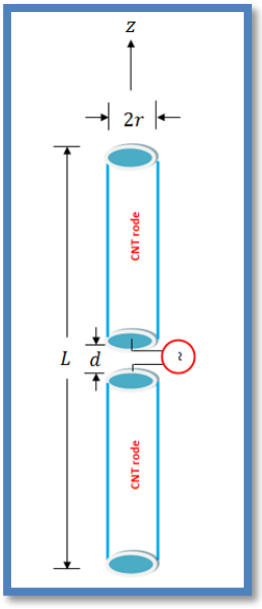

Fig 4: Geometry of the effective SWCNT or MWCNT antenna.

In fact, there is another way for dealing with the complex permittivity approach using CST software package, where the CNT material is set as a new material with normal type and Drude dispersion model. The value of epsilon infinity is one for all types of CNT material according to eqn. 22, where the term after the minus on the RHS will be finished when $\omega \gg \omega_p$. The value of plasma frequency is computed from eqn. 23, and the collision frequency is considered as the same value of the relaxation frequency.

Equations 24a and b state the relations between the real and imaginary parts of the relative complex permittivity, respectively, and both plasma and relaxation frequencies. Therefore, no difference between the two ways is expected, but the input data of the relative complex permittivity which is asked by the CST needs high accuracy and this may be not adjusted quietly. Therefore, feeding the input data of the plasma and relaxation frequencies when asked by the CST seems to be healthier.

By using of the concept of the solidity in Sec. 3, one can convert the electric and magnetic fields on the surface of original CNT (hollow cylinder) to the electric field $\boldsymbol{E}$ and magnetic field $\boldsymbol{H}$ in all regions of the solid cylinder model. The direction of $\boldsymbol{E}$ and $\boldsymbol{H}$ depends on the location of the CNT antenna in simulation environment. Using Maxwell's equations

$$\nabla \times \boldsymbol{H} = j\omega\varepsilon_c \boldsymbol{E} \quad \ldots(25a)$$

$$\nabla \times \boldsymbol{E} = -j\omega\mu \boldsymbol{H} \quad \ldots(25b)$$

will solve the CNT antenna problem, where ε_c is the relative complex permittivity defined by eqn. 20. Equations 25a and b may be solved by several methods. Choosing CST program as a numerical solver for these equations (after adjusting all parameters properly) will give more efficient results. The flowchart in Fig. 5 shows the process applied to CNT antenna using CST package.

5.1 RESONANCE FREQUENCIES

The SWCNT antenna is modeled with $L = 2\ \mu m$, $m = n = 40$, $v_F = 9.71 \times 10^5$ m/s, and $T = 300^0\ K$ as shown in Fig. 6. The plasma and relaxation frequencies are computed to be 192.9 and 0.1056 THz, respectively. The delta gap width (d) is chosen to be $2r$. The CNT is meshed tetrahedrally with mesh cells such that the convergence of S-parameters is satisfied with avoiding the long computational time.

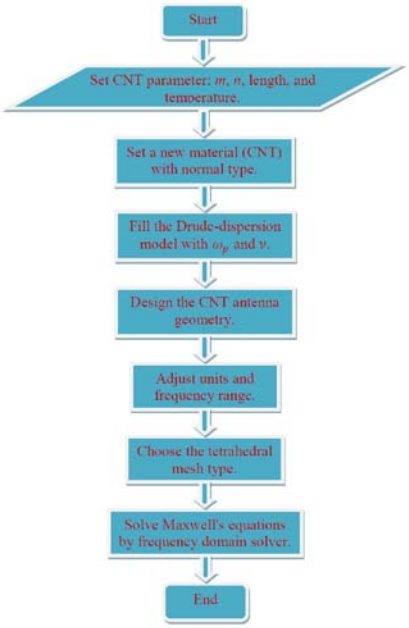

Fig 5: Flowchart for modeling CNT antenna using complex permittivity approach.

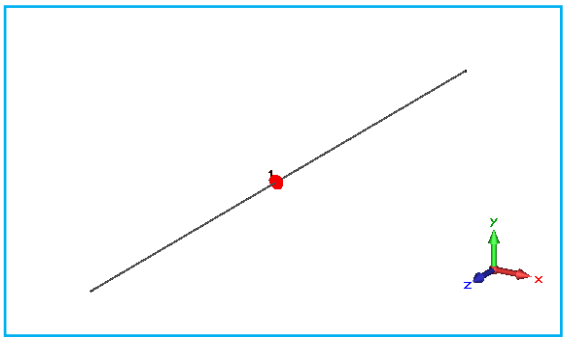

Fig 6: Modeled SWCNT antenna with $L = 2\ \mu m$ and $m = n = 40$.

The simulation results reveal that resonance frequencies occur at 891, 2400, 3680, and 4761 GHz. According to the relation $v_p = \lambda_{pc} f_r$ and $f_{r1} = 891$ GHz, the phase velocity is estimated to be 3.564×10^6 m/s $\cong 0.012\ c$ and this value is near to the expected phase velocity which is calculated according to the transmission line model as $v_p = 0.010\ c$, where c is the speed of light in free space. The phase velocities at the second, third, and fourth resonance frequencies are equal to $0.0160\ c$, $0.0163\ c$, and $0.01587\ c$, respectively. The four phase velocities (at resonance frequencies) seem to be close. Therefore, these values predict the proper working of the simulated SWCNT antenna.

The first resonance frequency of this antenna type is close to the collision frequency which may be the natural frequency that leads to the resonance case. In conventional antenna, the relaxation frequency is very high and this leads to the conclusion that the oscillation is independent of the collision frequency.

Figure 7 shows the variation of the relaxation and plasma frequencies with radius index. Both frequencies decrease sharply with m for $m < 50$. When m increases beyond 50, the variation of these two frequencies with m decreases and both frequencies approach saturated values when m tends to 200. At $m = n = 40$ and T = 300°K, $f_p = 192.9$ THz and $\nu = 0.1056$ THz. These values are to be compared with 38.58 and 0.02113 THz, respectively, when $m = n = 200$.

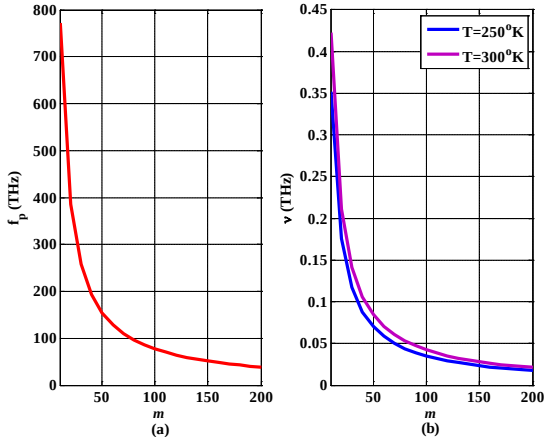

Fig 7 (a): Plasma frequency of a SWCNT versus m (b) relaxation frequency of a SWCNT versus m at difference temperature values.

The first resonance frequency is found to be a decreasing function of m as shown in Fig. 8. The resonance frequency decreases from 890 to 800 THz as m increases from 40 to 200. One of the main parameters that affects the resonance frequency is the relaxation frequency and this will be supported by $\nu = 6\mathrm{T}/r$ where T stays constant but r increases according to $r = (3/2\pi)\ bm$ (see Fig. 7b for variation of ν with m).

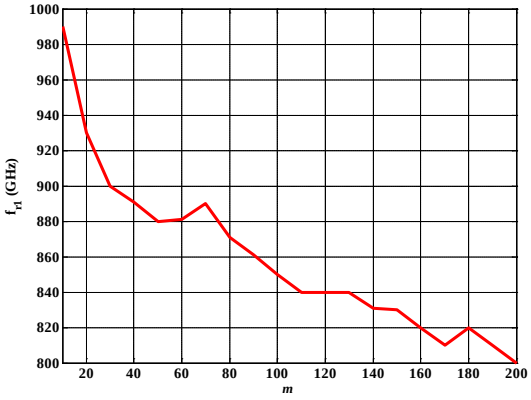

Fig 8: First resonance frequency versus m index for a 2 μm-armchair SWCNT antenna.

5.2 S_{11} PARAMETER

The S_{11} parameter or reflection coefficient of SWCNT antenna is shown in Fig. 9. The very small values of the reflection coefficient at the first and second resonance frequencies (< -30 dB) mean the SWCNT antenna has low reflection losses.

In this work, the adjustment of the input impedance of the discrete port Z_{inp} depends on getting a minimum value of the reflection coefficient or S_{11}

parameter. In the first time, the initial value of Z_{inp} has been estimated from Z_i and in each simulation run the seeking is toward the minimum value of S_{11}. The S_{11} parameter values of the simulated CNT antenna at

$$f_{r1},\ f_{r2},\ f_{r3} \text{ and } f_{r4}$$

are $-33.7,\ -33.3, -19.4$ and -18.4 dB, respectively. These small values are encouraging because more incident power will be transmitting and a little of it will be reflected. The termination of the CST program depends on the optimal value of S_{11} parameter. This property will accelerate the final result. In testing the complex permittivity approach, it is noted that any wrong change in the input data will make it impossible to get S_{11} parameter in this good range and this will give a good hoping for this approach.

From Fig. 9, the minimum values of the S_{11} parameter of the SWCNT antenna which occur at its resonance frequencies increase at high resonance frequencies. This does not exist in the conventional dipole antennas. This problem is due to the nature of the CNT conductivity, where the decrease in the CNT conductivity at high frequencies makes this material deviate from the state of good conductivity. This problem is naturally solved when the point of operation is far toward more high frequencies.

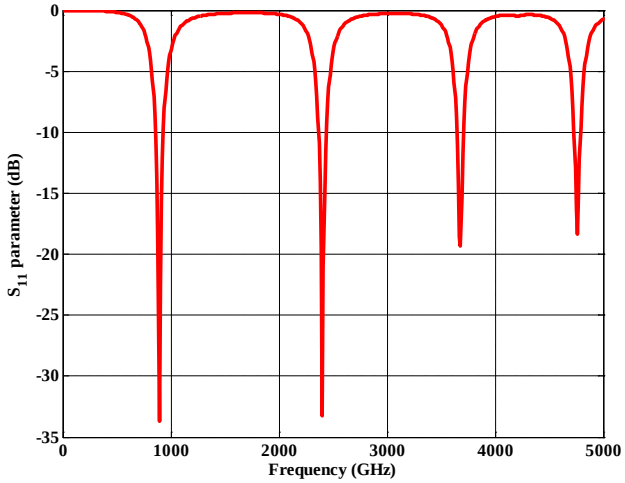

Fig 9: Magnitude of S_{11} parameter of a SWCNT designed with m=n=40 and $L = 2\mu m$.

Figure 10 shows the S_{11} parameter of a SWCNT antenna for several values of m. These results are estimated at the first resonance frequency and show that -40 dB $< S_{11} < -15$ dB for the range of $m < 200$ considered here. The estimated value may be considered as acceptable when dealing with this type of antennas where the sourced power must be small enough since it has a very low efficiency.

5.3 INPUT IMPEDANCE

As it is well known, the input impedance is considered as the main parameter in antenna design. A SWCNT antenna has input impedance Z_{in} which is quietly different from the classical antenna. The standard value of this impedance is 12.5 kΩ, but the classical antenna has a standard value of 50 Ω. Therefore, the task of adjustment this quantity is very important since any error will lead to destroy the transmitting or receiving signal. The matter of the power is sensitive here due to the very small values of the source power and high value of the input impedance of the CNT antenna Z_{in} with respect to the classical antenna.

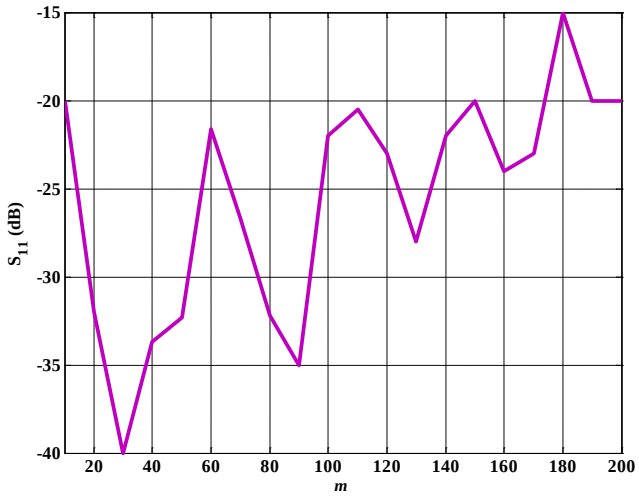

Fig 10: S_{11} parameters of a SWCNT antenna estimated at first resonance frequency for several values of m when $L = 2\mu m$.

The simulated real and imaginary parts of the input impedance are shown in Fig. 11. The first value of the antiresonance occurs at $f_1 = 1166$ GHz. The resonance frequencies occur at a travelling point from the capacitance to the inductance properties, but antiresonance frequencies occur at travelling from inductive to capacitive region. Therefore, in order to design a SWCNT antenna the resonance frequencies should be over antiresonance frequencies where the latter have large and rapid changes in values of the impedance. The values of the input resistance of the discrete port seem to be in the range of the quantum resistance and this value is compatible with the quantum resistance in the nanoelectronics [4], [7] where the CNT antenna is to be matched with it. Therefore, in order to make the SWCNT antenna work properly the impedance matching issue must be taken carefully to avoid the high input impedance which may not be satisfied in nanoelectronics, and at the same time, the large values may make deviation in the optimal initial values which speed up the running of CST. It is noted during the simulation of the CNT antenna by CST that one of the main parameters that accelerates the solution is the initial value of the input impedance. For example, if the

input impedance of the discrete port is chosen to be greater than 20 kΩ then no good results are obtained. The reason is that the CST is a numerical solver whose convergence speed depends on the good estimation of the initial values. Therefore, after choosing the initial value of the input impedance of the discrete port, depending on the calculated input impedance of the SWCNT transmission line (eqn. 13), the input impedance of the discrete is found to be 4.04 kΩ. One of the main advantages of this approach over referring references is its capability of computing the input impedance of the discrete port that is connected to the CNT antenna because this feature is very important during the designing any type of antennas.

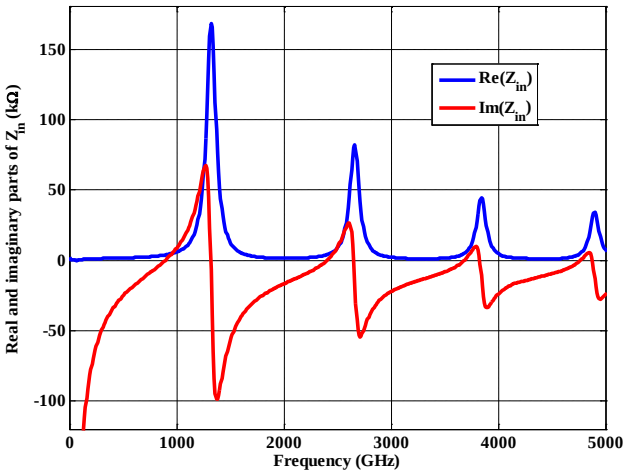

Fig 11: Input impedance of a SWCNT designed with $m = n = 40$ and $L = 2\ \mu m$.

The input impedance of the discrete port Z_{inp} versus several values of the armchair SWCNT diameters is shown in Fig. 12. Here, a SWCNT of length 2 μm is simulated using the complex permittivity approach. Figure 12 shows decrease in the values of Z_{inp} as the value of m increases. Therefore, as in the classical antennas, SWCNT must operate under matched condition which can be achieved by varying of (m, n) as well as the CNT length.

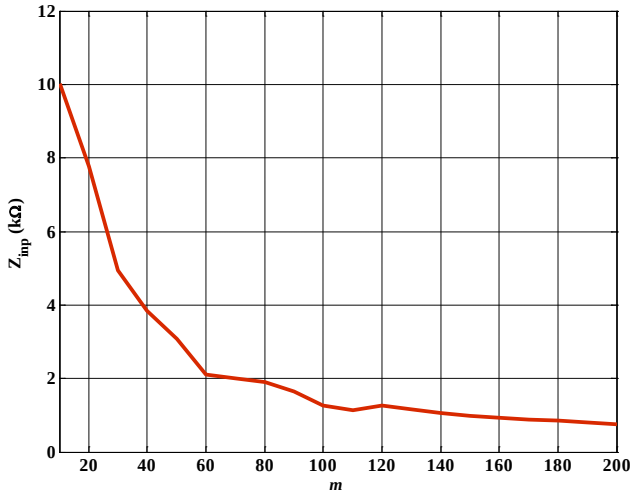

Fig 12: Input impedance of the discrete port versus $m = n = 40$ index for 2 μm armchair SWCNT antenna.

Figure 13 shows the input resistance of the SWCNT antenna for $m = n = 40, 50,$ and 60 simulated using the complex permittivity approach where the peaks change increasingly with different values of m. The input reactance is shown in Fig. 14 and it states the increasing in the reactance peaks as in the input resistance. The increase in the peaks of input resistance and reactance with m is due to the wide bandwidth which is set by CST, where the frequency domain solver needs setting in narrow bandwidth in order to give more accurate results. The wide band width has been chosen for seeing at least four resonance frequency regions.

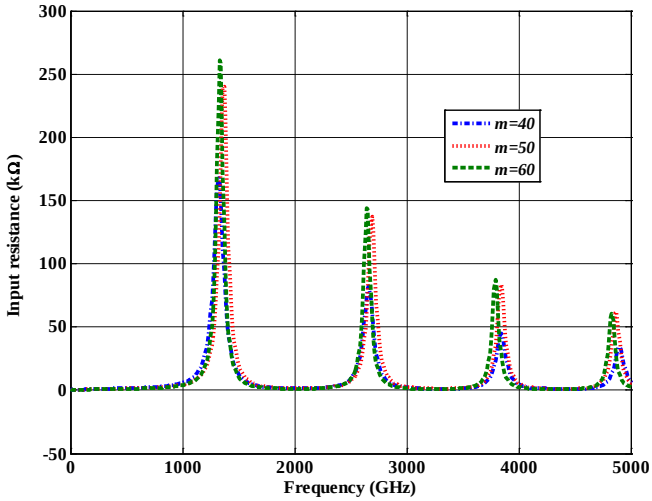

Fig 13: Input resistance of a SWCNT antenna for several $m = n$ values and $L = 2\ \mu m$.

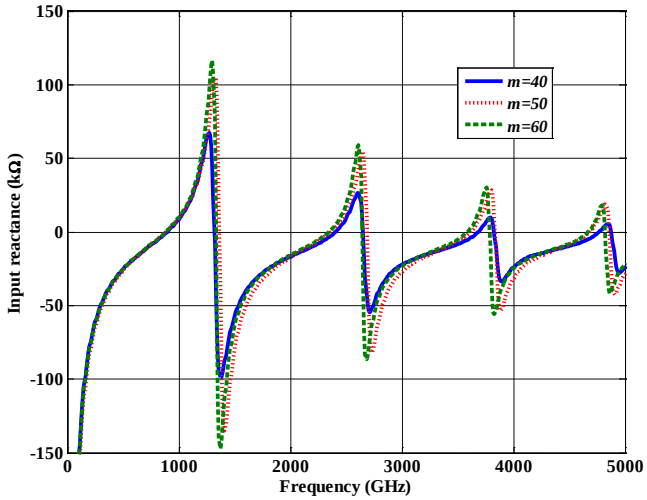

Fig 14: Input reactance of a SWCNT antenna for several $m = n$ values and $L = 2\ \mu m$.

5.4 RADIATION PATTERN, GAIN, AND EFFICIENCY

The radiation pattern (directivity) of the SWCNT antenna at the resonance frequencies is depicted in Fig. 15. On the other hand, the maximum values of the directivity as a function of frequency are shown Fig. 16. The low values of the directivity of Fig. 15 are interpreted by Fig. 16 where the maximum value of the directivity at frequency 891 GHz is 0.27. In moment, the directivity is enhanced in the other resonance frequencies as shown in Fig. 15b, c, and d. The best value of the directivity is found at $f_{r3} = 3680$ GHz which is equal to 1.68. This value can be compared with the directivity of the conventional dipole antenna which is 1.64. Therefore in order to obtain a CNT working with a maximum directivity, the first resonance frequency does not satisfy this requirement, i.e. another frequency must be sought such that the directivity and matching should be satisfied.

Figure 16 explains that the maximum directivity is not obtained at one of the resonance frequencies. The reason for this phenomenon is the conductivity which makes the SWCNT a propagation filter with high pass filter mode, where there is a relation between the directivity and electric field which is related to the conductivity by Ohm's law. At the same time, the high frequency values of the directivity are about 1.6 which is considered as the maximum value of the directivity of a classical dipole antenna.

The realized gain of the simulated antenna is shown in Fig. 17. Four peak gain values are shown whose frequency location coincides to some extent, with the four resonance frequencies shown in Fig. 9. The gain of a SWCNT is very low as expected in Ref. [8] since the antenna is designed with a very small radius with respect to the length. In other words, this antenna is electrically very thin according to $r \ll \lambda$ condition. Therefore, an agreement about this problem must be obeyed.

In order not to waste more time, the efficiency is considered as a copy of gain because of unity value of the directivity. The efficiency parameter is considered as the master feature in the antenna properties if the matter of power is considered. Since the total efficiency η_T is approximately equal to the radiation efficiency η_r (see Table 2), then the SWCNT antenna does not suffer from the reflection efficiency η_f where $\eta_T = \eta_f \eta_r$ and $\eta_r = \eta_d \eta_c$. Here η_d and η_c are dielectric and conduction efficiencies, respectively [17]. However, the antenna suffers from the low radiation efficiency as mentioned before. Also, the radiation efficiency can be written in the form $\eta_r = R_r/(R_r + R_L)$, where R_r and R_L are the radiation and losses resistances, respectively.

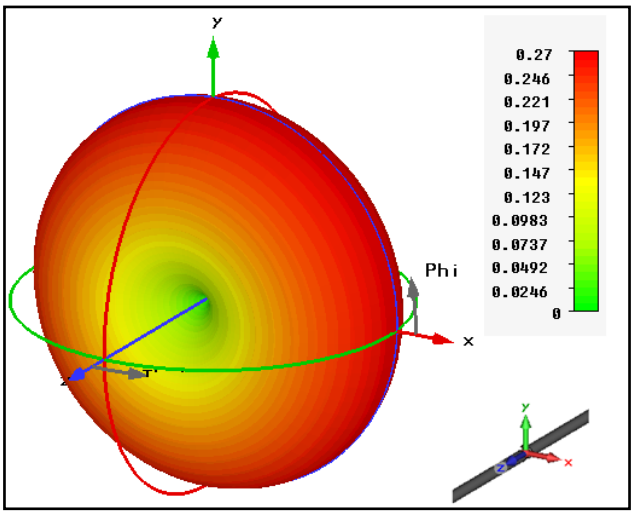

(a)

Fig 15: Radiation pattern for a SWCNT designed with $m = n = 40$ and $L = 2\ \mu m$ at (a) $f_{r1} = 891$ GHz (b) $f_{r2} = 2400$ GHz (c) $f_{r3} = 3680$ GHz (d) $f_{r4} = 4761$ GHz.

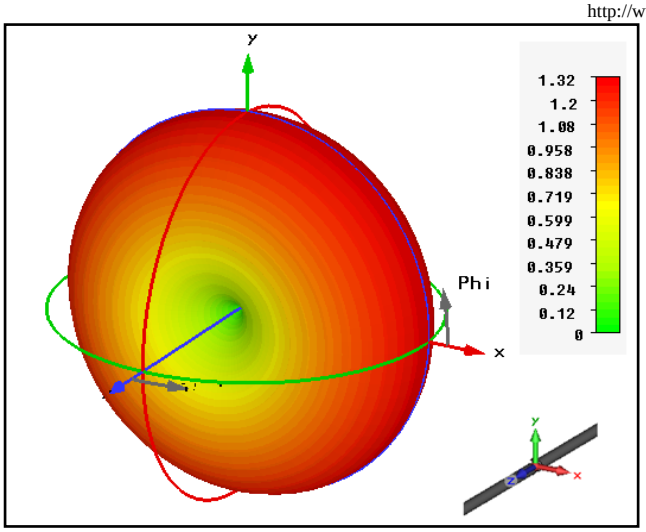

(b)

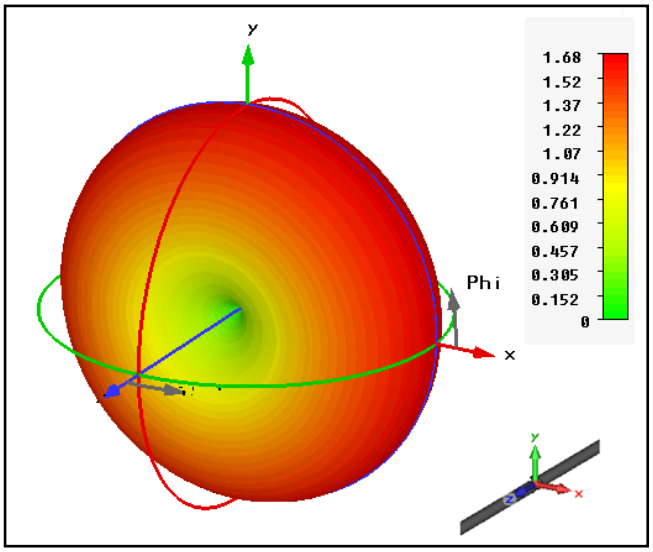

(c)

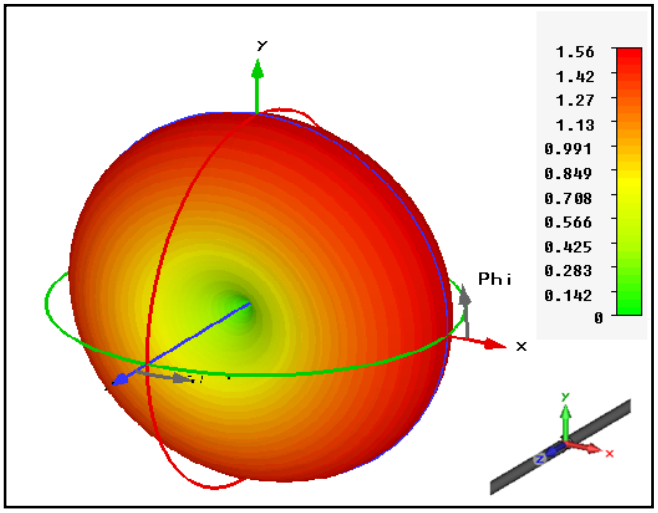

(d)

Fig 15 (Continued)

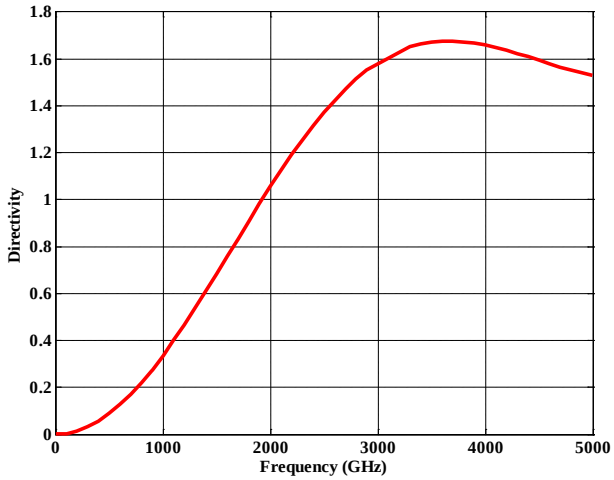

Fig 16: Directivity versus frequency for a SWCNT antenna designed with m=n=40 and L= 2 μm.

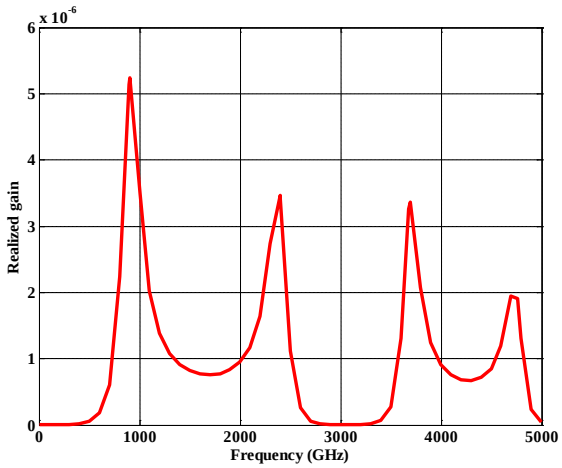

Fig 17: Realized gain versus frequency for a SWCNT antenna having $m = n = 40$ and L= 2 μm.

Table 2: Gain, radiation efficiency, and total efficiency at the resonance frequencies for a SWCNT antenna designed with $m = n = 40$ and $L = 2\ \mu m$.

Resonance frequency f_r (GHz)	Gain G	Radiation efficiency η_r	Total efficiency η_T
891	5.25×10^{-6}	1.904×10^{-5}	1.903×10^{-5}
2400	3.50×10^{-6}	2.603×10^{-6}	2.602×10^{-6}
3680	3.40×10^{-6}	1.972×10^{-6}	1.949×10^{-6}
4761	1.92×10^{-6}	1.241×10^{-6}	1.232×10^{-6}

6. SIMULATION OF MWCNT ANTENNAS

As in SWCNT antenna, the complex permittivity approach is used to simulate a MWCNT antenna using CST software package. This type of antennas can be constructed according to the number of shells in each MWCNT material. In real world, a MWCNT antenna consists of many parts and each part is called a SWCNT. In the environment of simulation, the MWCNT antenna is simulated by considering one equivalent part which is called an effective MWCNT antenna. In other words, the conductivity of the overall MWCNT is modified to be an effective conductivity (eqn. 17). Therefore, the final geometry is a MWCNT dipole antenna that is similar to the SWCNT dipole antenna but with mostly different parameters. Figure 18 shows the geometry representation of a MWCNT dipole antenna positioned along z-axis and built by CST package.

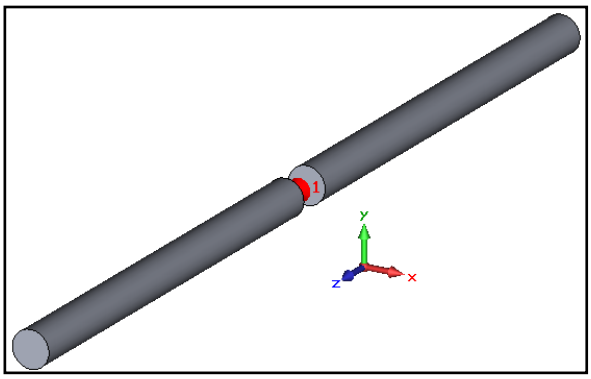

Fig 18: Geometry representation of a MWCNT dipole antenna built by CST package.

A number of MWCNT dipole antennas are simulated here, each with a different number of shells (N). The shell number $N = 5$ means that the MWCNT dipole antenna consists of 5 SWCNTs each inside the other. The inner SWCNT starts with dual index $m = n = 5$, the dual index of the second SWCNT is 10, and so on. Finally, the outer SWCNT will have $m = n = 25$. The same thing is valid for $N = 10, 15, 20, 25,$ and 30. This scenario of increasing the tube shells has been made by [13]. The results of simulated MWCNT dipole antennas of $2\ \mu$m length with several shell numbers are shown in Table 3. It is clear from this table that as the number of shells increases then the first resonance frequency f_{r1} shifts forward since the conductivity is increasing with N. On other hand, the plasmon wave number k_{pc} decreases. Therefore, the free space wave number k_0 becomes as the dominant factor in (k_0/k_{pc}) term. Whenever $k_0 > k_{pc}$, then the unusual low resonance frequency will be terminated and a MWCNT antenna seems to be a classical antenna. Therefore, a compromised solution must be made through designing a MWCNT antenna. The sharp decrease in the input impedance of the discrete port Z_{inp} with N is deduced from eqn. 17 or 18. The summation in eqn. 17 will increase the conductivity as N increases. The low effect of radiation resistance in CNT is due to the small radius which makes the input impedance of CNT line nearly alike to the input impedance of the CNT antenna.

Figure 19a and b shows the input resistance and input reactance, respectively, versus frequency for a MWCNT antenna simulated with $L = 2\ \mu$m and $T = 300^{o}K$. At the peak values, the resonance state is achieved. As in SWCNT antenna, the values of the input impedance of the MWCNT antenna are still very large. This makes the thinking with the antiresonance regions impossible. The justification which has been mentioned about the antiresonance in SWCNT antenna can be also applied to the MWCNT antennas.

Table 3: Results of simulated MWCNT dipole antenna of $2\ \mu$m length and several shell numbers.

N	f_r (GHz)	Z_{inp} (kΩ)	D	η_T
5	921	7.209	0.288	1.21×10^{-5}
10	1250	2.249	0.502	3.338×10^{-5}
15	1511	1.204	0.692	6.551×10^{-5}
20	1700	0.773	0.835	1.000×10^{-4}
25	1881	0.546	0.970	2.000×10^{-4}
30	2041	0.409	1.085	2.300×10^{-4}

The S_{11} parameter is considered as one of the main parameters used to distinguish between antennas performance. This performance is shown in Fig. 20. In this figure, S_{11} spectra are plotted for N=5, 10,…, 30. When the number of shells increases, the first resonance moves gradually to upper frequencies. When $N = 5$, the lowest first resonance frequency is attained and within the frequency range there are three resonance frequencies. In the case of N=10, 15, and 20, the number of resonance frequencies is two. Finally, there is one resonance frequency when N=25 and 30. Thus, the preferred region of operation depends on the demand and this must be confirmed by the number of shells.

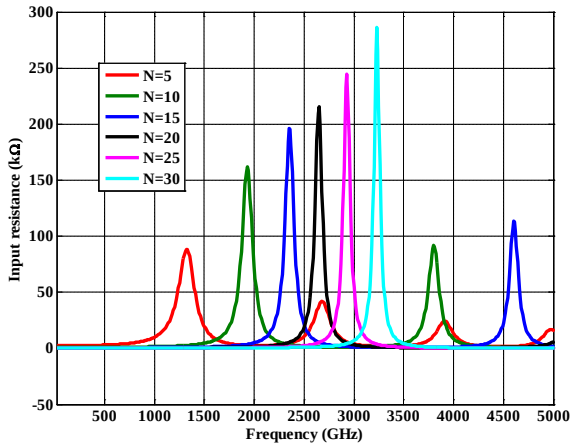

(a)

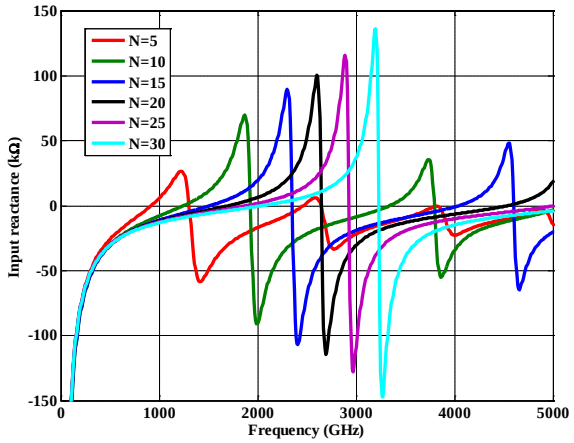

(b)

Fig 19: Input resistance (a) and input reactance (b) of a 2μm MWCNT dipole antenna length with various values of shell number (N).

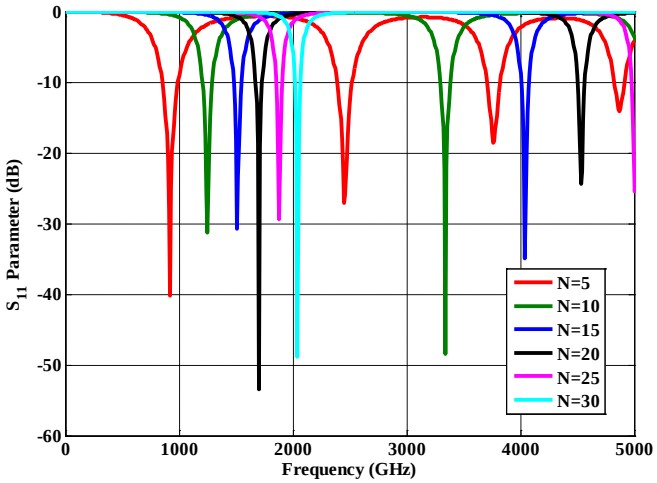

Fig 20: S_{11} parameter of a 2μm MWCNT dipole antenna length with various values of number of shells.

The directivity D and efficiency of MWCNT antenna appear to be adjusted to the ideal case as N is enlarged. This will keep away from the problem of low directivity at the first resonance frequency. More details on the directivity are depicted in Fig. 21 which shows the directivity does not efficiently changes with N. As long as the directivity stays constant and at the same time the efficiency increases then the gain will be increased as predicted by $G = \eta_T D$.

The radiation patterns for the MWCNT antenna simulated at the first resonance frequency for different values of N and the results are shown in Fig. 22. In the case of $N = 5$, the maximum value of the directivity is 0.288. As it is expected, the maximum value of the directivity is improved when N increase to become 1.085 at $N = 30$ as shown in Table 3.

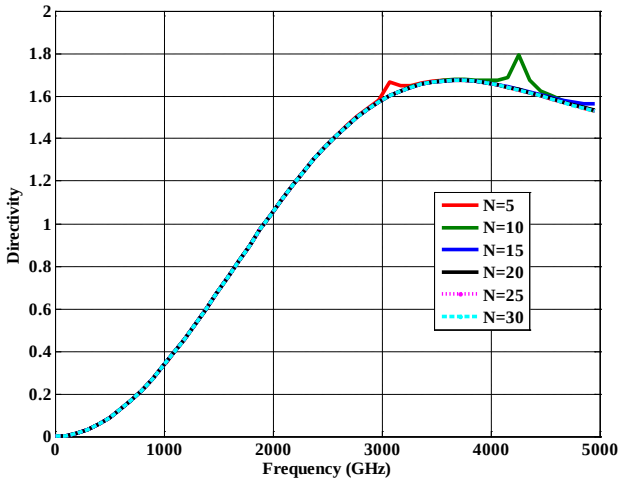

Fig 21: Directivity versus frequency of a 2μm MWCNT dipole antenna length with various values of number of shell.

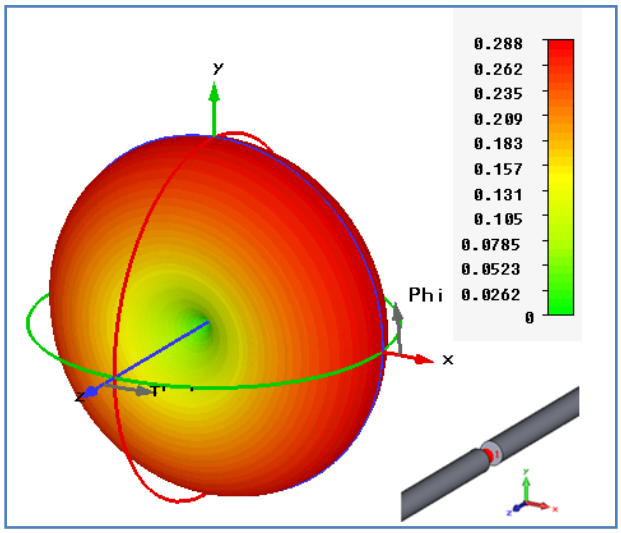

(a)

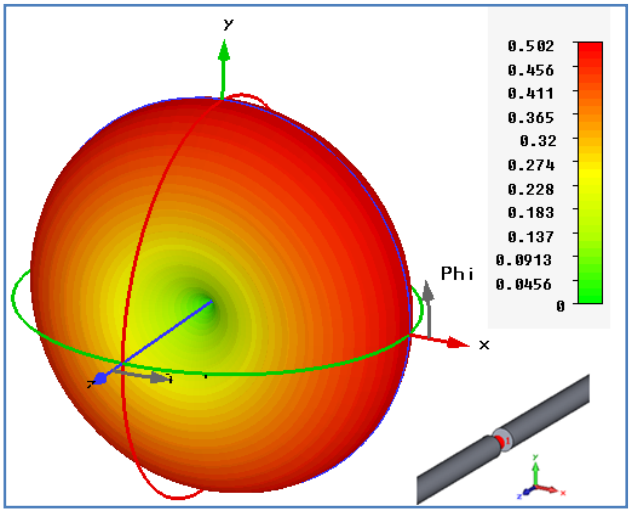

(b)

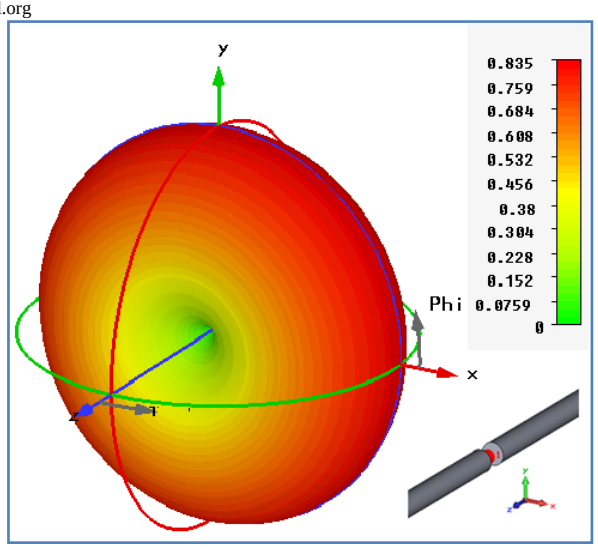

(d)

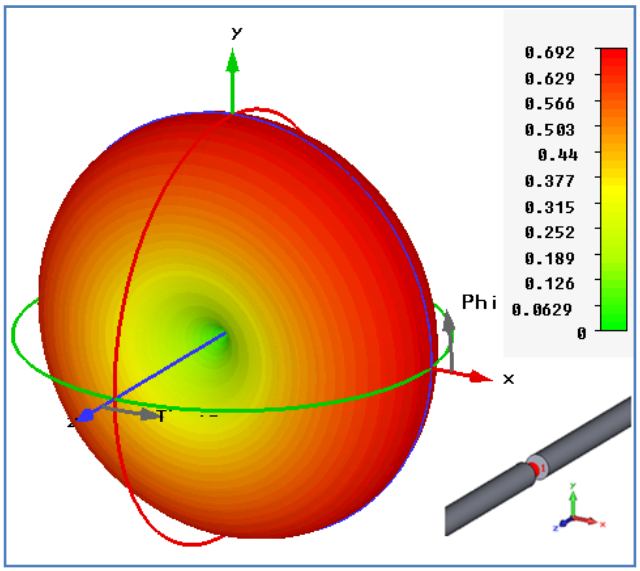

(c)

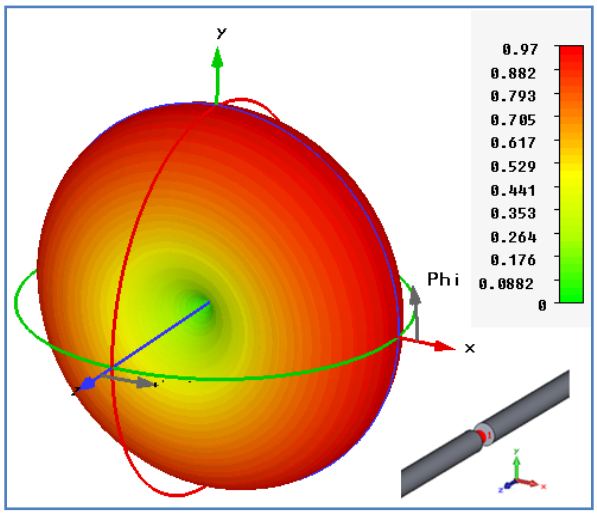

(e)

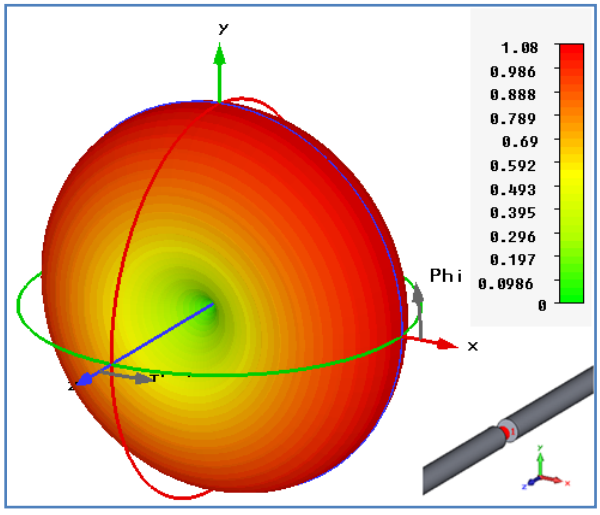

(f)

Fig 22: Radiation pattern for a MWCNT designed with $L = 2\ \mu m$ and (a) N = 5 (b) N = 10 (c) N = 15 (d) N = 20 (e) N = 25 (f) N = 30.

Fig 22: (Continued)

For the purpose of comparison between the SWCNT and MWCNT antennas, consider a SWCNT antenna having $m = n = 150$ and MWCNT antenna having $N = 30$ where the outer SWCNT has $m = n = 150$. Assume that both antennas have the same length which is equal to 2μm. Table 4.3 summarizes the main performance results deduced at the first resonance frequency for each antenna.

As a simple comparison with a SWCNT antenna, the MWCNT offers best performance if the issue of the low resonance frequency with respect to the electrical length is not taken into consideration. The prominent feature over a SWCNT antenna is the modification in efficiency and subsequently the gain is improved.

Table 4: Results of comparison between SWCNT and MWCNT antennas having the same outer radius.

Parameters	SWCNT	MWCNT
f_{r1} (GHz)	831	2041
Z_{inp} (kΩ)	0.992	0.409
S_{11} (dB)	-20	-49
η_r	7.112×10^{-5}	2.300×10^{-4}
η_T	7.036×10^{-5}	2.300×10^{-4}
D	0.2375	1.0850
G	1.668×10^{-5}	2.5×10^{-4}

7. SIMULATION OF BUNDLE CNT ANTENNAS

The Bundle CNT antenna that is modeled in CST can be described as aggregation of a SWCNT lines positioned along z-axis and arranged in a rectangular form to become a rectangular bundle CNT (RBCNT) antenna as illustrated in Fig. 23. The distance between adjacent SWCNTs is chosen to be 1nm and the length of each SWCNT is set to $2\ \mu$m and radius index of $m = n = 40$. Two square contacts are placed in the feeding region each with thickness equal to r and the length of the discrete port is $2r$. The contact is placed in this shape is to make a discrete port touch all tubes. The simulation frequency range is set to $1 - 5000$ GHz in order to cover at least the first resonance frequency band. Several values of the number of bundles are chosen in the simulation in order to inspect carefully the properties of a RBCNT antenna.

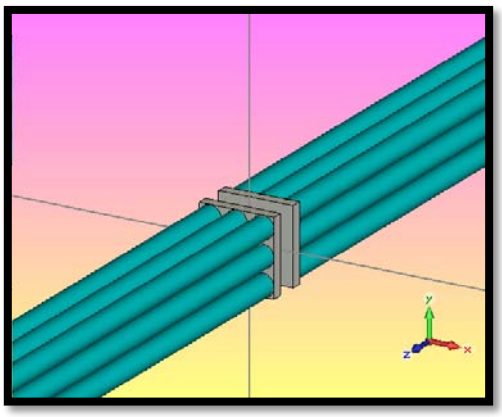

Fig 23: A rectangular bundle CNT antenna with N=9.

Initially, S_{11} parameter of a RBCNT antenna is set to the optimal value by varying the input impedance of the discrete port Z_{inp} until the agreement between this value and the input resistance of the antenna at a frequency where minimum of S_{11} is obtained. Figure 24 shows the S_{11} characteristics of a RBCNT antenna simulated using CST with the number of SWCNTs $N = 1, 4, 9, 16,$ and 25. Minimum value of the S_{11} parameter can be satisfied when N increases and this will lead to shifting up the resonance frequency as shown in Fig. 24 and Table 5. From this table, the input impedance of the discrete port decreases when N is increased because of increasing the antenna material conductivity by N. The case of $N = 25$ makes the RBCNT antenna moves toward the world of classical antennas at least at matching point where the input resistance of the classical antenna is $50\ \Omega$. Therefore, a small change in N may lead to a high change in the input impedance of the discrete port. Hence, the geometry must be changed according to the main specifications. The new structure may be a strip or cylindrical CNT antenna.

Table 5: Performance parameters of RBCNT antenna designed with different values of N.

N	f_r (GHz)	$f_{M,G}$ (GHz)	Z_{inp} $(k\Omega)$	G
1	815	800	0.4707	3.5×10^{-6}
4	1950	999	0.8060	1.0×10^{-4}
9	2950	2998	0.3280	7.0×10^{-4}
16	3725	3697	0.2020	2.0×10^{-3}
25	4816	4796	0.1250	4.0×10^{-3}

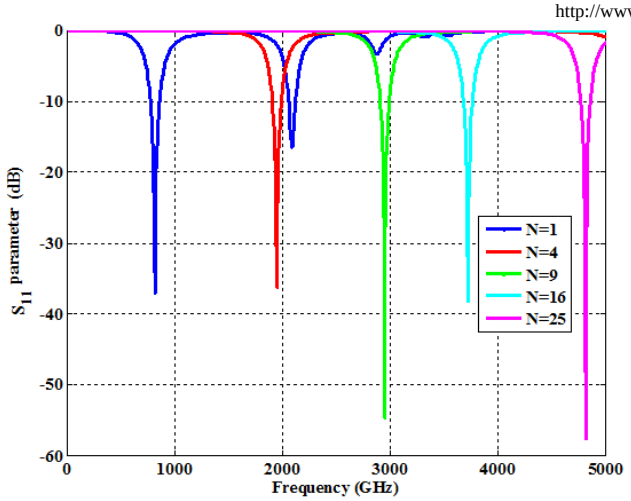

Fig 24: S_{11} parameter of the RBCNT antenna for several numbers of SWCNTs, N.

The radiation pattern of a RBCNT antenna having $N = 25$ is shown in Fig. 25. This figure shows that the directivity stays in the range of 1.64 (directivity of the conventional antenna). Therefore, no problem about the directivity is of concern.

The maximum value of realized gain at $\varphi = 0$ is calculated by taking N as independent parameter and the results are shown in Fig. 26. Note that the gain is modified as long as N is large. The frequencies at maximum gain $f_{M,G}$ and f_r are listed in Table 5.

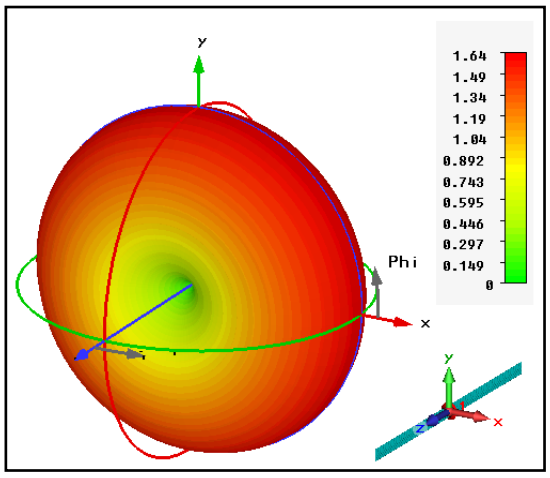

Fig 25: Radiation pattern of the RBCNT antenna for $N = 25$ and $f_{r1} = 4816$ GHz.

The simulation results related to the case of varying the dual index of each SWCNT in the RBCNT antenna of $N = 16$, while keeping the same separation distance between two SWCNTs as used in the previous RBCNT antenna, is illustrated in Fig. 27. This figure shows the dependence of S_{11} parameter on the frequency. The value of first resonance frequency decreases when m increases. This makes the entire SWCNT governs the properties of a RBCNT as well as N. Also, the input impedance of the discrete port Z_{inp} decreases with increasing the peak of the realized gain as shown in Table 6. From this table, Z_{inp} seems to approach the value of the input impedance of the classical antenna and makes Z_{inp} of the RBCNT unaffected by the quantum resistance. At the same time, the first resonance frequency is still in the range of plasma frequency. Hence, the RBCNT antenna may be considered as a compromise solution between the CNT and the classical antennas. Note that the peak of maximum gain at $\varphi = 0$ increases without increasing N, therefore, in order to modify the efficiency of a RBCNT antenna, a little of bundle element is enough with increasing the radius of each SWCNT element for the purpose of enhancement of gain and efficiency.

Table 6: First resonance frequency, input impedance of the discrete port, and peak of maximum gain of a RBCNT antenna with various m=n values and N=16.

Radius m=n	f_r (GHz)	Z_{inp} (Ω)	Gain Peak
40	3725	202	0.0017
60	3585	134	0.0025
80	3460	101	0.0029
100	3380	81	0.0034

8. CNT CONTACT

One of the main problems of CNT antenna is the contact of this type of antenna with the external world [18], [19], [20]. The small hollow geometry of CNT makes the connection more difficult. Therefore another solid material is necessary as an interface and should be chosen carefully such that it does not affect the main properties of the SWCNT antenna. Firstly, gold and copper are chosen in this work as metal contacts between the CNT rod and the feeding point. The length of the contact L_c must be as short as possible in order to make the current on CNT having enough time to oscillate sinusoidally with respect to the contact material. To address this issue, the SWCNT is modeled in CST environment using the complex permittivity approach with the following parameters: $L = 4\ \mu$m, $d = 2r$, $T = 300^0$ K, and $m = n = 100$. The reason for changing the length of the CNT antenna from $2\ \mu$m to $4\ \mu$m is to make the ratio of the contact length to antenna length as small as possible. Several values of contact length are taken and the results are compared with a CNT antenna designed without contact (the discrete port is connected directly to the CNT rods). Figure 28 shows the effective SWCNT antenna with a metal contact which is modeled in CST environment.

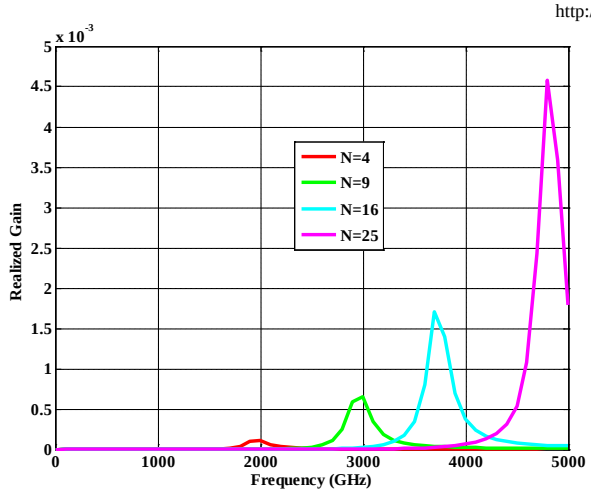

Fig 26: Maximum value of realized gain at φ =0, for various N.

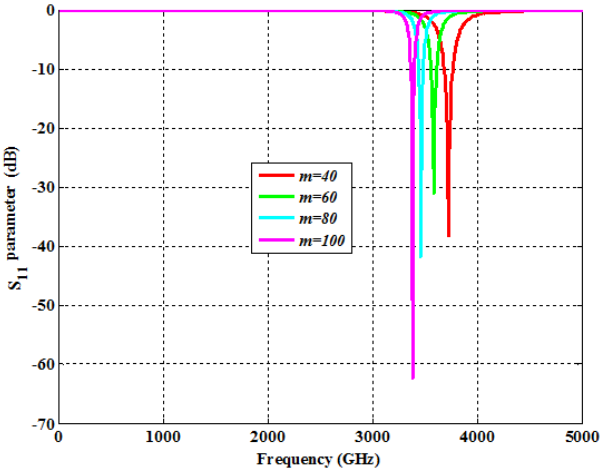

Fig 27: S_{11} parameter of a RBCNT antenna with various m.

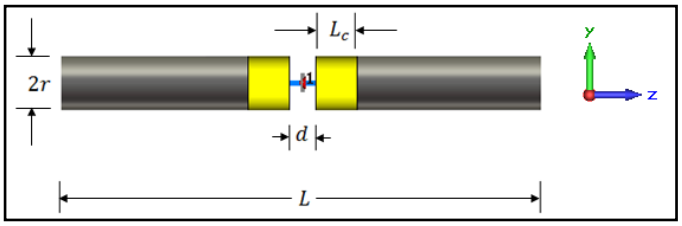

Fig 28: Geometry representation of the simulated SWCNT antenna with a metal contact.

When the length of SWCNT antenna increases from 2 μm to 4 μm, the first resonance frequency decreases. Therefore, the frequency band is set from 0 to 2500 GHz instead of 0 to 5000 GHz. Within this frequency range, the input impedance of the discrete port Z_{inp} is computed for several values of the contact length L_c. It is expected that when L_c increases then the first resonance frequency also increases due to the effect of copper (or gold) which has relaxation frequency much greater than that of the SWCNT. Several values of L_c are chosen and the related input impedance of the discrete port Z_{inp} and the first resonance frequencies f_r for each case are computed as shown in Figs. 29 and 30, respectively. The results indicate that Z_{inp} decreases with the contact length. This is because of the effect of quantum resistance which has large value with respect to the reciprocal of the conductivity for copper or gold contacts. The cause of increase in the values of the first resonance frequency is the effect of relaxation frequency in SWCNT where it is much smaller than the relaxation frequency in nanowires (copper or gold). As a result, CNT antenna can change its properties according to the design environment, for example by adding an external material to the contact point with different lengths.

It is worth noting here that there is a small effect variation between using copper or gold contact on the values of Z_{inp} but there is no change is noticed in the resonance frequency. This makes a free choose of the material type. Because of the effect of copper or gold contact, the two materials are used to design an antenna having a length of 4 μm and radius 6.78 nm. Figure 31 shows the S_{11} parameters for the copper and gold antenna which seem to be near to each other with respect to CNT antenna. The copper- and gold-contact antennas resonate at 55.73 and 54.92 THz, respectively. The SWCNT antenna with the same geometry parameters but without contact resonates at 441 GHz. The input impedances of the discrete port of copper-and gold-contact antennas are found to be 1.19 and 1.17 kΩ, respectively, and for a contactless SWCNT antenna is 3.44 kΩ. Therefore, in each case the contacted CNT tries to change its properties toward that of an antenna designed from the contact material.

9. FEEDING CNT ANTENNA WITH CNT TRANSMISSION LINE

One of the main design specifications is connecting the CNT antenna with the external world. In this work, the CNT antenna is proposed to be connected with a two-wire transmission line (TL) and this transmission line is assumed to have the same properties of the antenna (i.e., CNT TL) as shown in Fig. 32. In this figure, the length of the TL (L_T) is equal to L/32 for the purpose of viewing. Several values of L_T have been chosen as: L, L/2, L/4, L/8, L/16, and L/32. The length and radius of a SWCNT antenna are set to L=2 μm and r=2.71 nm, respectively.

Figure 33 shows the S_{11} characteristics of the simulated SWCNT antenna with different TL lengths. For TL length L_T= L, the lowest first resonance frequency is obtained and the following f_r is at L_T= L/2, and so on.

Therefore, the resonance frequency of the SWCNT antenna depends on the length of the feeding TL, where $f_r = 815$ GHz for a SWCNT antenna simulated without TL and $f_r = 291$ GHz at $L_T = L$. This high difference makes the issue of matching the CNT antenna with the TL more essential. Also, Z_{inp} can be changed but not rapidly (decreasing or increasing) as f_r increases where its values alternate at nearest values as shown in Table 7. Here, let the input impedance of the SWCNT antenna be termed $Z_{inp,SW}$ and the characteristic impedance of the SWCNT TL as $Z_{o,SW}$, where $Z_{o,SW} = {Z_{inp}}^2 / Z_{inp,SW}$. Thus, the characteristic impedance of the SWCNT TL can be calculated as $Z_{o,SW} = 2.31\ \text{k}\Omega$ for $L_T = L$, where $Z_{inp,SW} = 4.706\ \text{k}\Omega$ for all TL lengths.

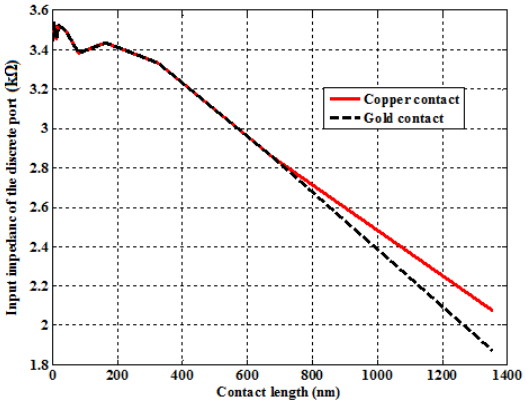

Fig 29: Input impedance of the discrete port versus contact length of a SWCNT antenna with different material contacts.

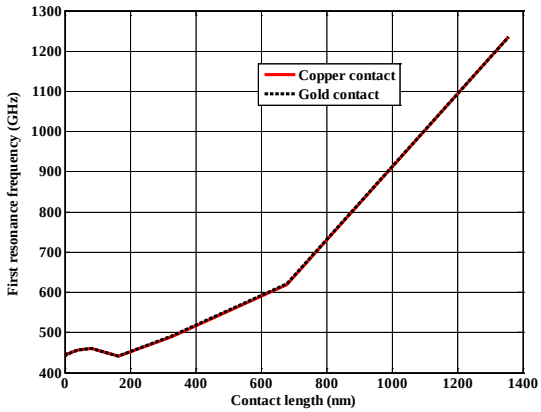

Fig 30: First resonance frequency of a SWCNT antenna versus contact length.

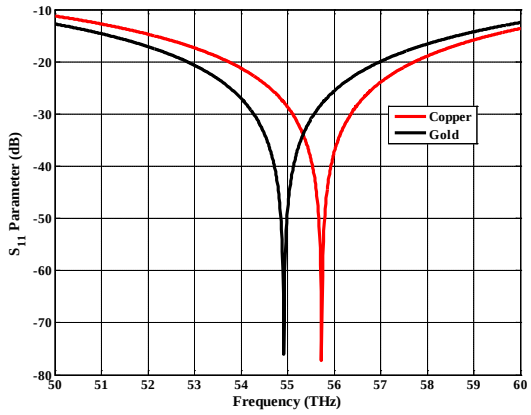

Fig 31: S_{11} parameter of copper and gold antennas.

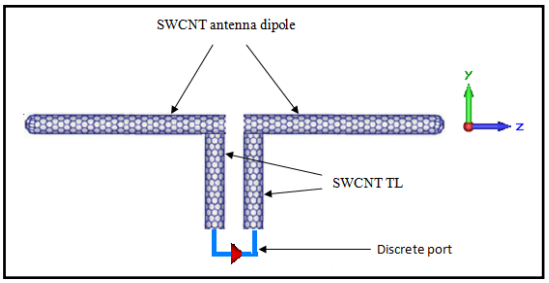

Fig 32: SWCNT antenna connected with SWCNT transmission line.

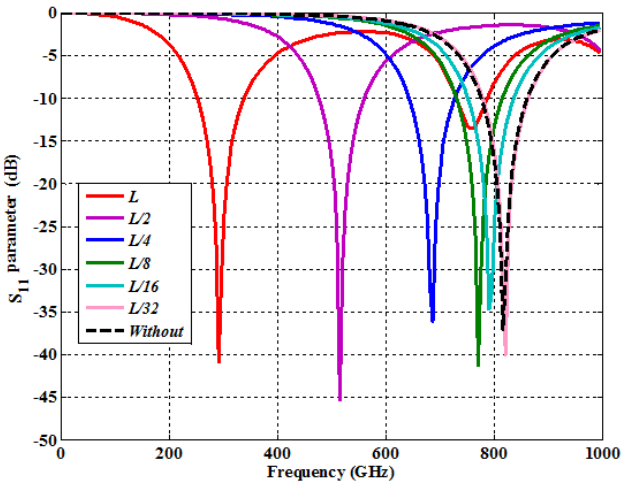

Fig 33: S_{11} parameter of a SWCNT antenna connected with a SWCNT transmission line having various lengths.

Table 7: First resonance frequency and input impedance of the discrete port of a 2 μm SWCNT antenna connected with a SWCNT transmission line of various lengths.

Transmission line length L_T (μm)	First resonance frequency f_{r1}(GHz)	Input impedance of the discrete port Z_{inp} (kΩ)
2.0000	291	4.512
1.0000	516	3.215
0.5000	686	3.523
0.2500	770	4.250
0.1250	791	4.225
0.0625	810	4.579
Without	815	4.706

10. CONCLUSIONS

Theoretical investigation has been carried out for predicting the radiation characteristics of various configurations of carbon nanotube antennas. Simulation results related to single-wall, multi-wall, and bundle CNT dipole antennas have been presented. The investigation reveals the following main findings

a. The concept of the effective conductivity of CNT material, which takes into account the frequency dependent complex permittivity, is an efficient tool to model various CNT antenna configurations using commercial software package.
b. CNT antennas exhibit multiband operation and this property is more emphasized when loop or helical configurations are used.
c. The gain and efficiency of the SWCNT dipole antenna are very small which can be enhanced when the dipole is redesigned using MWCNT or bundle CNT structures. The improvement increases with number of shells and number of SWCNT elements incorporated in the design.
d. Metal contact affects the performance of the CNT antennas and may lead to performance degradation. This degradation can be overcome by feeding the antenna with CNT transmission line.

REFERENCES

[1] Y. Wang, Q. Wu, W. Shi, X. Sun, and T. Gui, "Radiation Properties of Carbon Nanotubes Antenna at Terahertz/Infrared Range", International Journal of Infrared and Millimeter Waves, Vol. 29, No. 1, PP. 35–42, November 2007.

[2] A. Kleschenkov, A. Lerer, V. Makhno, P. Makhno, O. Labunko, "Electrodynamic Analysis of Carbon Nanotube Antenna", 12th International Conference on Mathematical Methods in Electromagnetic Theory, June 29 – July 02, 2008, Odesa, Ukraine.

[3] M. Dresselhaus, G. Dresselhaus, and A. Jorio, "Unusual Properties and Structure of Carbon Nanotubes", Annual Review of Materials Research Vol. 34, PP. 247-278, March 2004.

[4] G. Hanson, "Fundamental Transmitting Properties of Carbon Nanotube Antennas", IEEE Transactions on Antennas and Propagation, Vol. 53, No. 11, PP. 3426-3435, November 2005.

[5] J. Hao and G. Hanson, "Electromagnetic Scattering from Finite-Length Metallic Carbon Nanotubes in the Lower IR Bands", Physical Review B, Vol. 74, No. 035119, PP. 1-6, July 2006.

[6] G. Hanson, "Current on an Infinitely-Long Carbon Nanotube Antenna Excited by a Gap Generator", IEEE Transactions on Antennas and Propagation, Vol. 54, N0. 1, PP. 76-81, January 2006.

[7] J. Hao and G. Hanson, "Infrared and Optical Properties of Carbon Nanotube Dipole Antennas", IEEE Transactions on Nanotechnology, Vol. 5, No. 6, PP. 766-775, November 2006.

[8] P. Burke, S. Li, and Z. Yu,"Quantitative Theory of Nanowire and Nanotube Antenna Performance", IEEE Transactions on Nanotechnology, Vol. 5, No. 4, PP. 314-334, July 2006.

[9] J. Hao and G. Hanson, "Optical Scattering from a Planar Array of Finite-Length Metallic Carbon Nanotubes", Physical Review B, Vol. 75, No. 165416, PP. 1-7, April 2007.

[10] S. Maksimenko, G. Slepyan, A. Nemilentsau, and M. Shuba, "Carbon Nanotube Antenna: Far-Field, Near-Field and Thermal-Noise Properties", Physica E, Vol. 40, PP. 2360–2364, 2008.

[11] N. Fichtner, X. Zhou, and P. Russer, "Investigation of Carbon Nanotube Antennas Using Thin Wire Integral Equations", Advances in Radio Science, Vol. 6, PP. 209–211, 2008.

[12] A. Nemilentsau, G. Slepyan, S. Maksimenko, A. Lakhtakia, and S. Rotkin, "Scattering of The Near Field of an Electric Dipole by a Single Wall Carbon Nanotube", Journal of Nanophotonics, Vol. 4, No. 041685, PP. 1-23, April 2010.

[13] J. Berres and G. Hanson, "Multiwall Carbon Nanotubes at RF-THz Frequencies: Scattering, Shielding, Effective Conductivity, and Power Dissipation", IEEE Transactions on Antennas and

Propagation, Vol. 59, No. 8, PP. 3098-3103, August 2011.

[14] S. Choi and K. Sarabandi, " Performance Assessment of Bundled Carbon Nanotube for Antenna Applications at Terahertz Frequencies and Higher", IEEE Transactions on Antennas and Propagation, Vol. 59, No. 3, PP. 802-809, March 2011.

[15] G. Hanson, "A Common Electromagnetic Framework for Carbon Nanotubes and Solid Nanowires—Spatially Dispersive Conductivity, Generalized Ohm's Law, Distributed Impedance, and Transmission Line Model", IEEE Transactions on Microwave Theory and Techniques, Vol. 59, No. 1, PP. 9-20, January 2011.

[16] K. Zhang and D. Li, "Electromagnetic Theory for Microwaves and Optoelectronics", Springer-Verlag Berlin Heidelberg, 2nd edition, New York, 2008.

[17] C. A. Balanis "Antenna Theory Analysis and Design", John Wiley and Sons, 3rd edition, USA, 2005.

[18] J. Zhang, N. Xi, H. Chen, K. Lai, G. Li, and U. Wejinya, "Design, Manufacturing, and Testing of Single-Carbon-Nanotube-Based Infrared Sensors", IEEE Transactions on Nanotechnology, Vol. 8, No. 2, PP. 245-251, March 2009.

[19] H. Chen, N. Xi, K. Lai, C. Fung, and R. Yang, "Development of Infrared Detectors Using Single Carbon-Nanotube-Based Field-Effect Transistors", IEEE Transactions on Nanotechnology, Vol. 9, No. 5, PP. 582-589, September 2010.

[20] M. D'Amore, M. Sarto, and A. Tamburrano, "Fast Transient Analysis of Next-Generation Interconnects Based on Carbon Nanotubes", IEEE Transactions on Electromagnetic Compatibility, Vol. 52, No. 2, PP. 496-50, May 2010.